Hematopoietic stem and progenitor cells are present in healthy gingiva tissue

JEM Journal of Experimental Medicine

BRIEF DEFINITIVE REPORT

Hematopoietic stem and progenitor cells are present in healthy gingiva tissue

Siddharth Krishnan[1], Kelly Wemyss[1], Ian E. Prise[1], Flora A. McClure[1], Conor O'Boyle[1], Hayley M. Bridgeman[1], Tovah N. Shaw[1,2], John R. Grainger[1], and Joanne E. Konkel[1]

Hematopoietic stem cells reside in the bone marrow, where they generate the effector cells that drive immune responses. However, in response to inflammation, some hematopoietic stem and progenitor cells (HSPCs) are recruited to tissue sites and undergo extramedullary hematopoiesis. Contrasting with this paradigm, here we show residence and differentiation of HSPCs in healthy gingiva, a key oral barrier in the absence of overt inflammation. We initially defined a population of gingiva monocytes that could be locally maintained; we subsequently identified not only monocyte progenitors but also diverse HSPCs within the gingiva that could give rise to multiple myeloid lineages. Gingiva HSPCs possessed similar differentiation potentials, reconstitution capabilities, and heterogeneity to bone marrow HSPCs. However, gingival HSPCs responded differently to inflammatory insults, responding to oral but not systemic inflammation. Combined, we highlight a novel pathway of myeloid cell development at a healthy barrier, defining a gingiva-specific HSPC network that supports generation of a proportion of the innate immune cells that police this barrier.

Introduction

Our understanding of how immune cells are tailored to barrier environments to support effective immunity has expanded substantially in recent years. In particular, we are developing a better understanding of the immune mechanisms reinforcing the integrity of the mucosal barrier surrounding the teeth, termed the gingiva (Moutsopoulos and Konkel, 2018). This is an important advance, as loss of appropriate immune control in the gingiva leads to the development of periodontitis, the most common chronic inflammatory disease of humans (White et al., 2012). This oral inflammatory disease poses a threat to overall systemic health, as it has been linked to the exacerbation of a plethora of other inflammatory conditions including cancer, cardiovascular disease, and rheumatoid arthritis (Atarashi et al., 2017; Konkel et al., 2019; Kostic et al., 2012). Thus, delineating the local signals tailoring immune cell development and function at the gingiva would not only promote the development of therapies for periodontitis, but could also have implications for the treatment of other inflammatory conditions.

Similar to other barriers, the gingiva is home to commensal bacteria that must be effectively restrained in its niche. Yet the gingiva is a unique barrier site with distinct innate cell dynamics. For example, neutrophils have previously been shown to be the largest population of innate mediators policing this site (Dutzan et al., 2016b), and it has been estimated that every minute, 30,000 neutrophils extravasate from the gingiva into the gingival sulcus, the external body space between the gingiva and the tooth (Schiött and Löe, 1970). Surprisingly, how innate immune populations are maintained at and effectively tailored to the gingiva has been minimally explored. One innate cell population that exhibits exquisite capabilities for local, tissue-specific adaptation are monocytes and their macrophage progeny (Lavin et al., 2014). As such, we aimed to delineate how these key immune cells were tailored to the gingival environment.

Although some macrophage populations are generated early in development and are locally maintained at barriers (Ginhoux and Jung, 2014), circulating monocytes are also recruited from the blood to barriers, where they differentiate into macrophages (Bain et al., 2013; Tamoutounour et al., 2013). Monocytes develop from bone marrow (BM)–resident hematopoietic stem cells (HSCs) in specialized niches via controlled differentiation of intermediate progenitor populations that lose self-renewing capacity and become more restricted to the monocyte lineage. Committed monocytes then enter the blood, where they circulate before recruitment to barrier sites (Guilliams et al., 2018). In contrast to this conventional pathway of monocyte development,

[1]Lydia Becker Institute of Immunology and Inflammation, Faculty of Biology, Medicine and Health, Manchester Academic Health Science Centre, University of Manchester, Manchester, UK; [2]Institute of Immunology and Infection Research, School of Biological Sciences, University of Edinburgh, Ashworth Laboratories, Edinburgh, UK.

Correspondence to Joanne E. Konkel: joanne.konkel@manchester.ac.uk.

here we show that a large population of Ly6C^{hi} monocytes in the gingiva arose via a nonconventional pathway and could be locally maintained. Importantly, we show that healthy, noninflamed gingiva contained monocyte progenitors and HSCs that could support the local production of not just monocytes, but other short-lived myeloid cell populations. Previous studies have shown that at steady state, a scarce population of circulating hematopoietic stem and progenitor cells (HSPCs) constantly surveys tissues and can trigger local hematopoiesis upon activation (Massberg et al., 2007). Stress, inflammation, and infection elicit retention of HSPCs in tissues and drive initiation of this extramedullary hematopoiesis (EMH; Griseri et al., 2012; Saenz et al., 2010), where the immune cells required to deal with the inflammatory challenge are generated outside of the BM environment. Contrasting with current understanding of hematopoiesis at barriers, here we outline the presence of HSPCs in healthy gingiva, in the absence of overt inflammation and/or tissue perturbation. Gingival HSPCs were capable of differentiating into numerous myeloid populations; in addition to monocytes, neutrophils and other innate cells resident in healthy gingiva could be locally maintained.

Our data demonstrate that HSPCs are present in healthy gingival tissue, which, as defined by single-cell RNA-sequencing (RNA-seq), are similar to those in the BM. Moreover, gingival HSPCs possess an in vivo reconstitution ability and differentiation potential similar to BM HSPCs. Despite this, gingiva and BM HSPCs respond differently to inflammatory challenge. Gingiva HSPCs respond to local, oral inflammatory stimuli but respond differentially to systemic inflammatory challenges that remodel BM HSPCs. Importantly, our data demonstrate a bifurcation of innate cell generation during health, outlining a novel pathway of innate cell generation that occurs in the gingiva.

Results and discussion

A large population of barrier-resident monocytes are present in healthy gingiva and exhibit unique developmental requirements

In contrast to the gastrointestinal (GI) tract and skin, where cells with a CD64^{+}MHCII^{hi} macrophage phenotype dominate, most lineage^{-}CD11b^{+} cells present in the gingiva exhibited a classic (Ly6C^{hi}) monocyte-like phenotype despite the absence of inflammation (Fig. 1 A and Fig. S1, A and B). A dominance of monocytes over macrophages was also seen by staining gingiva tissue sections for immunofluorescence (Fig. S1, C and D). This large putative Ly6C^{hi} monocyte population was not in the blood but the gingiva, as evidenced by minimal staining with anti-CD45 following i.v. antibody injection (Fig. 1 B; Anderson et al., 2014). A large monocyte population was also prominent in the gingiva of another inbred mouse strain, specifically Balb/c (Fig. S1 B). The Ly6C^{hi} population expressed monocyte/macrophage markers but exhibited a monocyte-like cell morphology distinct to that of purified gingival macrophages (Fig. S1, E and F). A defining feature of blood and BM Ly6C^{hi} monocytes is their capacity to differentiate into F4/80^{+} macrophages. Suggestive of their monocytic state, purified gingiva Ly6C^{hi} cells were able to differentiate into macrophages upon culture with M-CSF (Fig. S1 G). Moreover, genome-wide transcriptional profiling of these Ly6C^{hi} cells compared with monocytes in the BM, blood, skin, and GI tract further confirmed their monocyte identity, as they expressed genes associated with the monocyte rather than the macrophage lineage (Fig. S1 H; Ingersoll et al., 2010; Lavin et al., 2014; Mildner et al., 2017). Taken together, these findings demonstrate that a large population of monocytes is present in healthy gingiva.

Comparative analysis of the gingiva monocytes to those purified from other body sites revealed that monocytes in the gingiva were most similar to those in the BM, not other barrier sites (Fig. 1 C), with a distinct gene cluster consisting of genes up-regulated in only BM and gingival monocytes. This cluster (cluster VI) was enriched in cell cycle genes, such as *Cdk2*, *Cnn2a*, and *Mcm* family genes (Fig. 1 C) and gene ontology terms associated with cellular replication (Fig. 1 D), suggesting that at least a fraction of gingival monocytes, like in the BM (Hettinger et al., 2013; Mildner et al., 2017), retain proliferative capacity. Combined, these data outline a gingiva monocyte network that is starkly different from that at other barrier sites.

To further explore the development of gingival monocytes, we injected mice with a single dose of EdU and noted that, similar to BM monocytes, gingiva monocytes were rapidly labeled (Fig. 1 E). Gingiva monocytes were labeled before those in the blood, suggesting they were unlikely to seed this site via the established development route where monocytes traffic from the BM to blood before entering tissues. We also examined *Ccr2*$^{-/-}$ mice, which have reduced circulating Ly6C^{hi} monocytes due to defective exit from the BM, causing deficiencies in tissue-resident monocyte-derived populations (Serbina and Pamer, 2006). Gingiva monocytes were unchanged in these animals (Fig. 1 F), further suggesting a distinct developmental pathway for these cells.

We next used a head-shielded BM chimera approach to determine whether gingival monocytes could be locally maintained. Host mice were irradiated with their heads shielded by lead and then reconstituted with congenic BM. Following reconstitution, most monocytes in the blood were donor derived; however, more than half of gingival monocytes were host derived (Figs. 1 G and S1 I). These data indicated that ∼50% of Ly6C^{hi} monocytes in the gingiva could be locally maintained. This did not change with time: when head-shielded chimeras were examined at ∼20 wk after reconstitution, the same proportion of gingival monocytes were host derived (Fig. S1 J). This local maintenance of a large proportion of monocytes in the gingiva was unique to this barrier, as monocytes in the ear skin, another shielded site in these chimeras, were predominantly donor derived, similar to the blood (Fig. 1 G). Moreover, when we examined chimerism of monocytes in the lung of torso-shielded chimeras and GI tract of abdomen-shielded chimeras, similar to the ear skin, monocytes exhibited high levels of chimerism (Fig. S1 K), further highlighting the distinct developmental requirements of gingival monocytes relative to other barrier sites.

Monocytes are short-lived immune effectors, usually rapidly mobilized from the circulation to sites of inflammation;

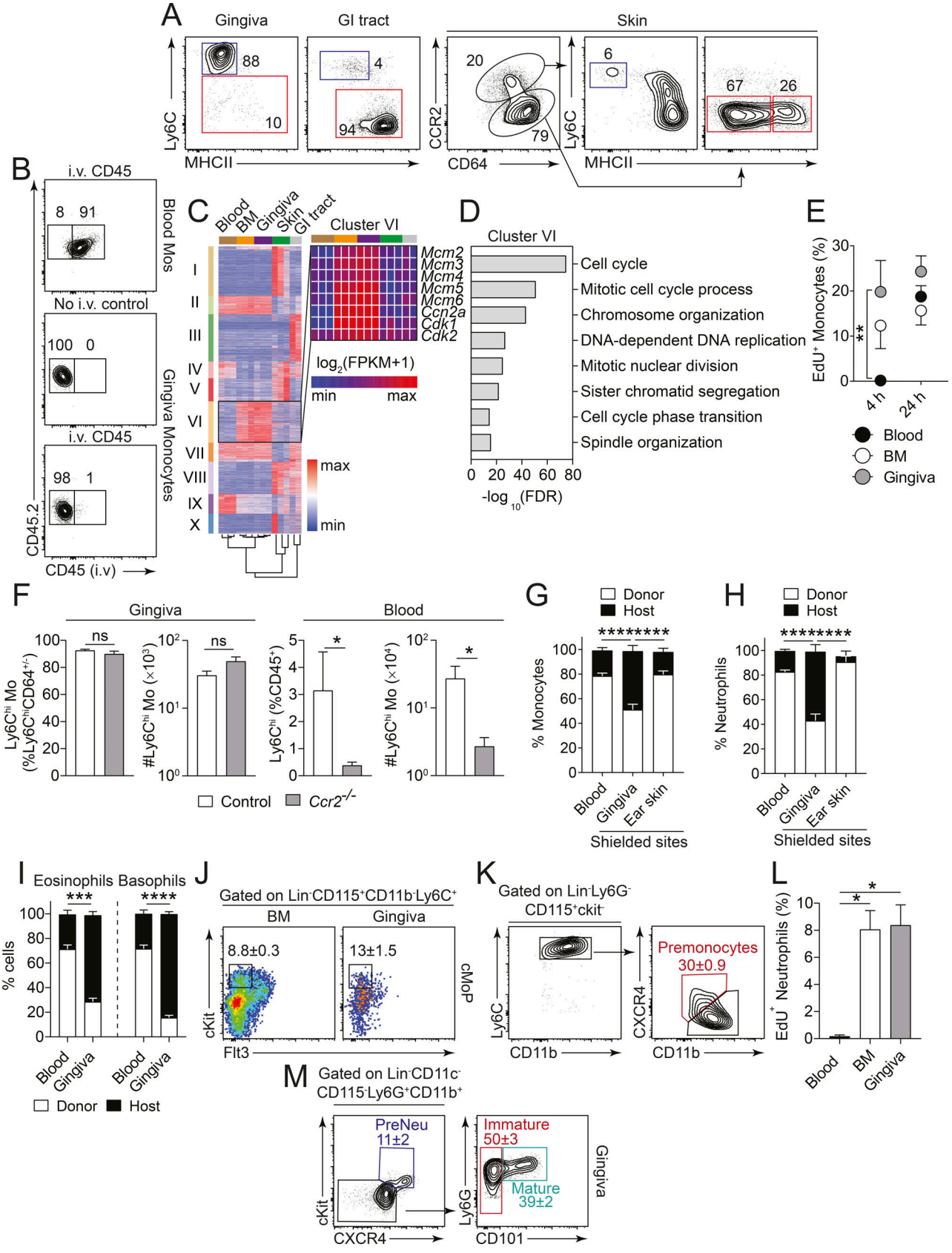

Figure 1. **A large population of monocytes is present in healthy gingiva. (A)** Representative FACS plots showing monocytes (blue gate) and macrophages (red gate) as a percentage of live CD45$^+$Lin$^-$CD11b$^+$Ly6C$^{+/-}$CD64$^{+/-}$ cells (excludes Ly6C$^-$CD64$^-$ cells) in the gingiva and GI tract. In the skin, they were similarly identified but were additionally CD24^{low}, and the Ly6C/CD64 was gated on CCR2. *n* = 6–13 mice per group. Lin = CD3ε, TCR-β, CD19, B220, NK1.1, Ter119,

Siglec F, and Ly6G. **(B)** Representative contour plots of monocyte (Mos) labeling with i.v. administered, fluorescently conjugated CD45 antibody in the gingiva and blood. *n* = 2–3 mice and representative of two independent experiments. **(C and D)** Monocytes were FACS purified from the blood, BM, gingiva, skin, and GI tract and analyzed by RNA-seq. *n* = 2–3 biological replicates per group. **(C)** Hierarchical clustering of the gene expression profile of monocytes from the indicated tissue sites. FPKM, fragments per kilobase per million mapped reads. **(D)** Pathway analysis of genes up-regulated by monocytes in the BM and gingiva identified in cluster VI by hierarchical clustering of their transcriptomic profiles using PANTHER and graphed according to enrichment score. FDR, false discovery rate. **(E)** Frequencies of monocytes in the blood, BM, and gingiva labeled by a single dose of EdU administered in vivo. *n* = 4 mice per group from two independent experiments. **(F)** Frequencies and total numbers of monocytes (Mo) in the gingiva and blood of control (white bars) and *Ccr2*$^{-/-}$ (gray bars) mice. *n* = 3–7 mice per group from two independent experiments. **(G–I)** Head-shielded BM chimeras were generated by irradiating CD45.2 (host) mice with their heads shielded by lead and reconstituting with CD45.1 (donor) BM. The proportions of donor-derived (white bar) and host-derived (black bar) monocytes (G), neutrophils (H), and eosinophils and basophils (I) were examined in the blood (non-shielded site) and the gingiva and ear skin (both shielded sites) at 11–12 wk after reconstitution. *n* = 6–11 mice per group from two to three experiments. **(J)** Representative pseudocolor plots identifying the common monocyte progenitor (cMoP) in BM and gingiva. *n* = 2–5 mice from two independent experiments. **(K)** Representative FACS plots identifying premonocytes in the gingiva. *n* = 6 mice from three independent experiments. **(L)** Frequencies of neutrophils in the blood, BM, and gingiva labeled by a single dose of EdU 24 h following administration. *n* = 4 mice per group from two independent experiments. **(M)** Representative FACS plots identifying preneutrophils and immature and mature neutrophils in the gingiva. *n* = 3–4 mice from two independent experiments. Data are presented as mean ± SEM on graphs and FACS plots. Statistical comparisons were performed using a two-way ANOVA with a Tukey's post hoc test (E and G–I), unpaired *t* test with Welch's correction (F, left panel), Mann–Whitney *U* test (F, right panel), and a one-way ANOVA with a post hoc Holm–Šídák test (L); ****, P < 0.0001; ***, P < 0.001; **, P < 0.01; and *, P < 0.05.

however, our data suggest a proportion of gingiva monocytes were locally maintained. Given that the composition of the gingival innate cell compartment is strikingly distinct from other barrier sites (Fig. S1 L), we next queried whether this was specific to this population or a feature of other short-lived immune effectors present in healthy gingiva. We first examined gingiva neutrophils in the head-shielded chimeras and saw that a substantial proportion of these cells were also host derived (Fig. 1 H). Again, this contrasted with what we saw in the ear skin of head-shielded chimeras, where neutrophils were mainly donor-derived, exhibiting the same chimerism as neutrophils in the blood (Fig. 1 H). Moreover, substantial proportions of other short-lived myeloid cells that could be identified in healthy gingival tissue, specifically eosinophils and basophils, were host derived in the head-shielded chimeras after reconstitution (Fig. 1 I).

Combined, these data suggest that myeloid populations present in healthy gingiva could be locally maintained, separate from BM input. However, the presence of a BM source within the skull could account for our findings, although this source would need to differentially replenish cells within the ear skin versus the gingiva (Fig. 1, G and H). To further examine possible local generation of these myeloid populations in the gingiva, we examined the larger populations of monocytes and neutrophils in more detail. Within the gingival monocyte population, in addition to some of these cells having proliferative capacity (Fig. 1 E), we could identify common monocyte progenitors and CXCR4^{+} premonocytes (Fig. 1, J and K; Chong et al., 2016). Along these lines, in gingival tissue, we could also identify populations of proliferating neutrophils (Fig. 1 L) and the recently defined populations of and pre- and immature neutrophils (Figs. 1 M and S1 M; Evrard et al., 2018). The presence of cells exhibiting phenotypes of earlier stages of monocyte and neutrophil development further indicated local development of these myeloid cells in healthy gingival tissue.

HSPCs are present in healthy gingiva

To further explore the possibility that gingiva myeloid populations could be locally generated, we assessed whether gingival tissue contained myeloid cell progenitors or HSPCs that could support this. Low numbers of circulating HSPCs constantly survey tissues and can trigger local hematopoiesis upon inflammation and infection, initiating EMH (Granick et al., 2012; Massberg et al., 2007). As such, few HSPCs are resident in healthy tissues at steady state. We isolated single-cell suspensions from gingiva and, strikingly, identified HSPCs in this tissue in the absence of overt inflammation (Fig. 2 A). This included not only specific innate cell progenitors such as myeloid progenitor cells (MyP; gated as Lin^{-}Sca-1^{-}cKit^{+}), common myeloid progenitors (CMPs), and granulocyte-monocyte progenitors, but also Lin^{-}cKit^{+}Sca-1^{+} (LSK) cells, multipotent progenitor (MPP) cells (LSK, CD48^{+}), and short- and long-term (LT) HSCs (Fig. 2, A–C; and Fig. S2 A). Barrier-resident HSPCs were not present in other healthy barriers examined (Fig. 2 D). Additionally, we also identified gingival HSPCs in Balb/c mice (Fig. S2 B). Importantly, the HSPCs identified were present within gingival tissue, and not blood contaminants, as they did not label with anti-CD45 injected i.v. (Fig. 2, E and F).

We have previously highlighted that local mechanical damage is a key modifier of gingival immunity (Dutzan et al., 2017; Krishnan et al., 2018), suggesting that steady state at the gingiva is distinct from steady state at other barriers, with the gingiva exhibiting signs of low-grade inflammation despite maintenance of health. As such, we examined whether elevated gingival damage could impact tissue-resident HSPCs. We assessed gingival HSPCs in mice maintained on normal or hardened chow diets (with mice on the harder diet experiencing elevated gingival damage during mastication). In mice experiencing elevated gingival barrier damage, there was an increase in the number of long-term HSCs in the gingiva (Fig. S2 C). These data suggest that the local damage experienced by the gingival barrier can modify the local HSPC network, but combined, our data importantly demonstrate that healthy, noninflamed gingival tissue houses a diverse population of HSPCs.

Gingival HSPCs are capable of hematopoietic reconstitution

To confirm that the HSPC populations we identified in healthy gingiva exhibited hematopoietic potential, we next dispersed

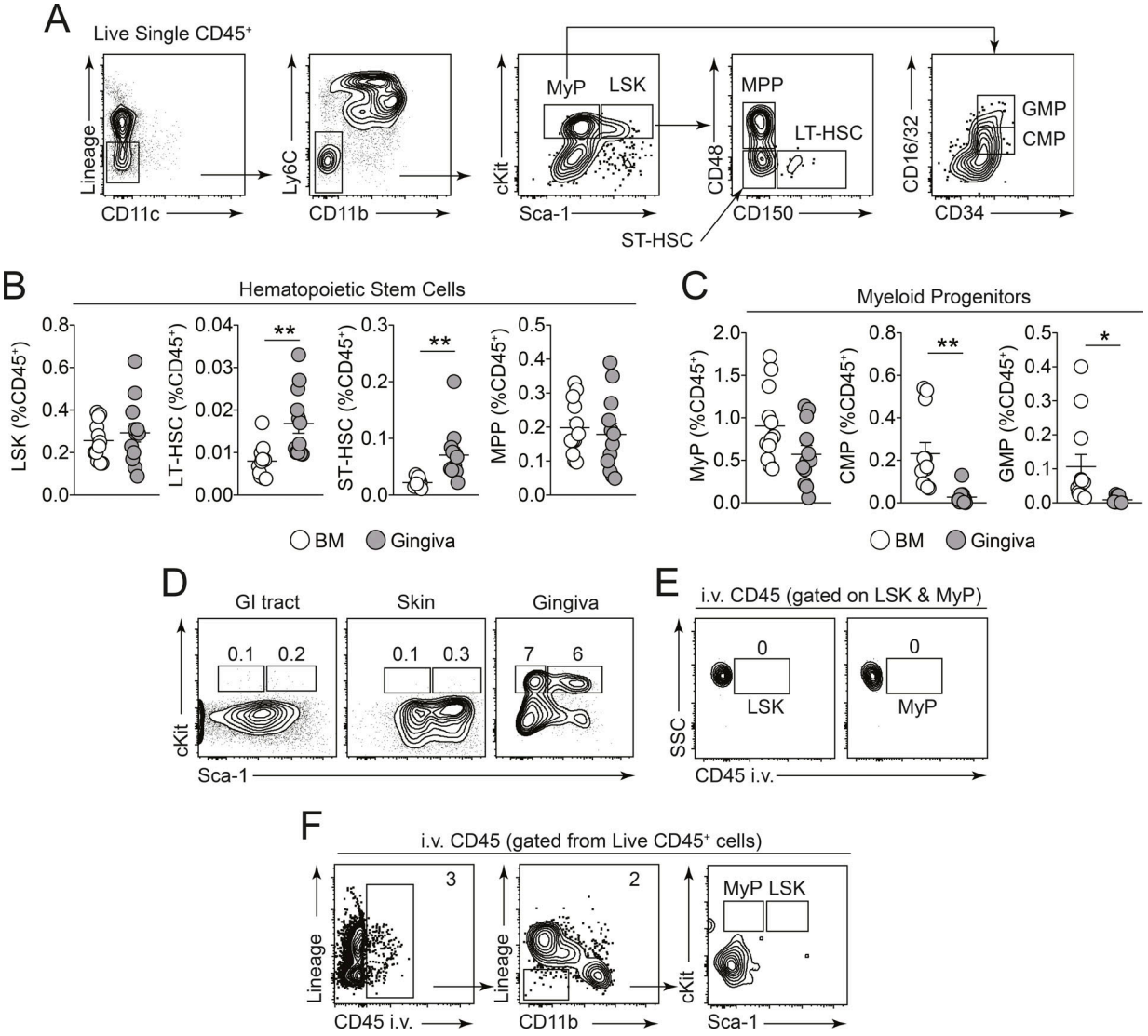

Figure 2. **HSPCs are present in healthy gingiva. (A)** Representative contour plots for the gating strategy to identify HSPCs in the gingiva. Lin = CD3ε, TCR-β, CD19, B220, NK1.1, Ter119, Siglec F, Ly6G, FcεR1α, CD11b, CD11c, and Ly6C. **(B and C)** Frequencies of HSCs (B) and MyP (C) in the BM and gingiva expressed as a percentage of total CD45+ cells. *n* = 12 mice per group from four independent experiments. ST-HSC, short-term HSC; GMP, granulocyte-macrophage progenitor. **(D)** Representative FACS plots showing HSPCs in the GI tract, skin, and gingiva. *n* = 3–6 from two independent experiments. Numbers show mean frequencies (among CD45+) and SEM. **(E and F)** Representative contour plots of gingiva HSPCs labeling with i.v. administered fluorescently labeled CD45 antibody. **(E)** Gating on LSK and MyP plots show staining for CD45 antibody injected i.v. **(F)** Gating on all cells staining positive for CD45 antibody injected i.v. and subsequent gating for LSK and MyP. Data are representative of two to three mice from three independent experiments. In all cases, numbers indicate percentage of cells in the gate. Data are presented as mean ± SEM. Statistical comparisons were performed using an unpaired *t* test with Welch's correction (B and C); **, P < 0.01; *, P < 0.05.

single-cell suspensions of gingiva tissue in MethoCult medium. Gingiva cells developed into CFU colonies, mainly of the granulocyte-macrophage phenotype (Fig. 3, A and B), indicating they possessed hematopoietic potential. Although the level of hematopoietic activity present in the gingiva was lower than that in the BM, it was substantially higher than that in other healthy barrier tissues, which possess little hematopoietic potential (Fig. S2 D). Flow-cytometric analysis of the colony-forming progeny generated following MethoCult culture of gingiva and BM preparations demonstrated the development of granulocytes and monocytes (Fig. 3 C). These data demonstrate that healthy gingival tissue houses cells with hematopoietic activity.

To explore the hematopoietic potential of gingiva relative to BM HSPCs, we purified LSK and MyP from both tissues by flow cytometry and cultured these cells in MethoCult medium. CFU activity per cell was similar for HSPCs sorted from the gingiva and BM (Fig. 3 D). Moreover, the progeny generated in these cultures were similar when comparing gingiva and BM isolated HSPCs (Fig. 3, E and F). Combined, these in vitro approaches confirm that healthy gingival tissue itself houses cells with hematopoietic activity and that the in vitro hematopoietic activity and differentiation potential of gingival HSPCs was similar to BM HSPCs. We next ascertained whether gingival HSPCs were capable of long-term multilineage reconstitution of hematopoiesis

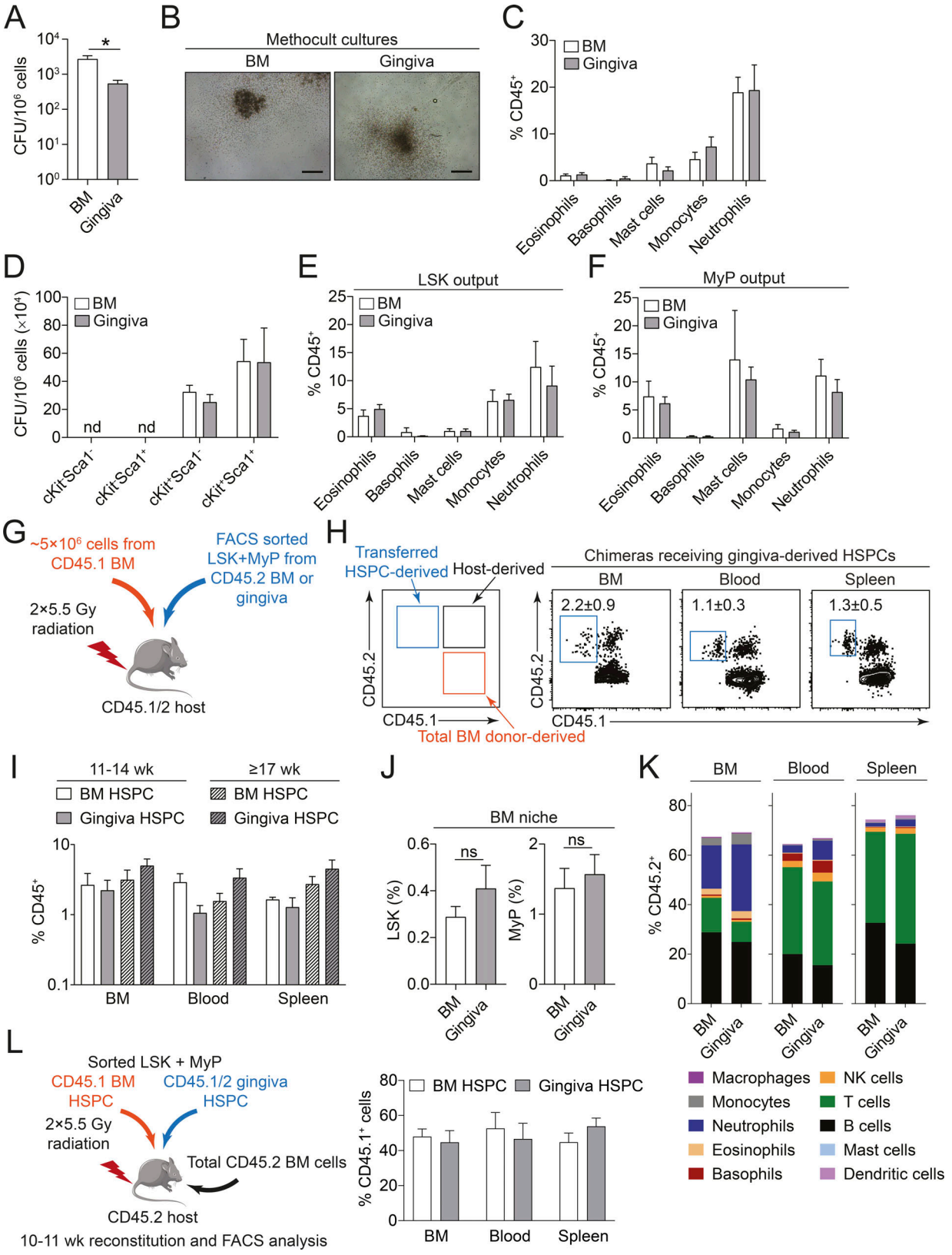

Figure 3. **Gingival HSPCs are capable of hematopoietic reconstitution. (A–C)** Single-cell suspensions from the BM (white bars) and gingiva (gray bars) were cultured in MethoCult medium for 10 d. **(A)** CFU activity from MethoCult cultures of total BM and gingiva tissue. **(B)** Representative photomicrographs of MethoCult colonies from cultures of single-cell preparations from BM and gingiva. Scale bar = 500 µm. **(C)** Quantification of the lineage output from MethoCult cultures of BM and gingiva preparations determined by flow cytometry. *n* = 4–12 per group from six experiments. **(D–F)** FACS-sorted hematopoietic progenitors were isolated from the BM and gingiva, and equal numbers of cells were seeded in MethoCult medium. **(D)** CFU activity of gingiva or BM FACS-sorted

cells. **(E and F)** Quantification of the lineage output from MethoCult cultures of FACS-sorted LSK (cKit$^+$Sca1$^+$) and MyP (cKit$^+$Sca1$^-$). Data representative of three independent experiments. **(G)** Schematic of the generation of whole-body chimeras. Anesthetized CD45.1/2 hosts were sublethally irradiated and received equal numbers of LSK + MyPs FACS sorted from the gingiva or BM of CD45.2 mice alongside total BM cells from CD45.1 mice. **(H)** Representative FACS plots identifying gingiva HSPC-derived CD45.2$^+$ cells within total CD45$^+$ cells (both CD45.1 and CD45.2) in the BM, blood, and spleen. **(I)** Quantification of BM and gingiva HSPC-derived cellular progeny in the indicated tissues expressed as a percentage of the total CD45$^+$ population, at early time points (11–14 wk, solid bars) and late time points (≥17 wk, hatched bars) after reconstitution. *n* = 5–12 mice/group from two to three independent experiments for each time point. **(J)** Frequencies of BM LSK and MyPs that were derived from BM-HSPCs or gingiva-HSPCs examined 11–14 wk after reconstitution. Data expressed as a percentage of total donor HSPC-derived cells. *n* = 5–6 mice per group from two independent experiments. **(K)** Lineage output of BM and gingiva HSPC-derived progeny in the BM, blood, and spleen at 11–14 wk after reconstitution, expressed as a percentage of total donor HSPC-derived cells. *n* = 5–6 mice per group from two independent experiments. **(L)** Left: Equal numbers of LSK + MyPs were sorted from the BM of CD45.1 mice and gingiva of CD45.1/2 mice and transferred into sublethally irradiated CD45.2 hosts who also received total CD45.2 BM cells. Mice were reconstituted for 10–11 wk, after which the proportion of BM- or gingiva-derived cells was analyzed by FACS. Right: Proportions among all CD45.1 cells of BM- and gingiva-derived progeny in the BM, blood, and spleen. *n* = 5/group from two independent experiments. Data are presented as mean ± SEM except in K, where mean frequencies of HSPC-derived progeny are plotted. Statistical comparisons were performed using an unpaired *t* test with Welch's correction (A and J), a two-way ANOVA with a post hoc Holm–Šídák test (C–F, K, and L), and Tukey's test (I); *, P < 0.05. We acknowledge Servier Medical Art (https://smart.servier.com) for cartoons used in this figure.

in vivo. LSK and MyP were collectively sorted from the gingiva and transplanted into sublethally irradiated, congenically distinct recipients alongside total BM cells from a third congenically distinct donor (Fig. 3 G). Equal numbers of LSK and MyP cells were also sorted from the BM and transferred in an identical way into recipients to assess the capabilities of gingival versus BM HSPCs. Following reconstitution, gingiva HSPC-derived cellular progeny were identified in all organs examined (Fig. 3, H and I; and Fig. S2, E and F) demonstrating that gingival HSPCs were capable of surviving and generating progeny when transferred into irradiated hosts. Gingival HSPCs were equally capable of reconstitution compared with BM HSPCs, as they generated a similar-sized population of CD45$^+$ cells; this was true whether examining engraftment at earlier (11–14 wk) or later (≥17 wk) time points (Fig. 3 I). In line with this, examining the HSPC-derived cells in the BM demonstrated a similar-sized population of LSK and MyP cells in the BM of mice that received HSPCs sorted from the gingiva and BM (Figs. 3 J and S2 G), demonstrating equally efficient colonization of, and survival within, BM niches. To determine the potential of the transferred HSPCs, we examined the cellular identity of their progeny. Focusing on the peripheral blood, BM, and spleen, multilineage reconstitution ability was seen for transferred HSPCs sorted from both BM and gingiva (Figs. 3 K and S2 H). Moreover, similar frequencies of the different immune lineages were generated by HSPCs from both sources (Figs. 3 K and S2 H). These data highlight that the transferred HSPCs possessed similar reconstitution capabilities and differentiation potentials when they colonized the BM. This was further confirmed in competitive BM chimeras, where congenically distinct HSPCs from the BM and gingiva were co-transferred into the same host. Examined 10–11 wk after reconstitution, there was no difference in reconstitution capacity of HSPCs from either source (Fig. 3 L), and similar multilineage reconstitution was also seen (Fig. S2 I). Combined, these data demonstrate that healthy, noninflamed gingiva contains HSPCs capable of colonizing the BM niche and reconstituting multiple hematopoietic lineages.

Differential responsiveness of the BM and gingival HSPC niches

Our data highlighted a surprising similarity between the functional potentials of HSPCs in the gingiva and BM. To better understand the similarity between the HSCs from the gingiva and BM, we sort purified lineage-depleted LSK plus MyP (CD45$^+$Lin$^-$cKit$^+$) cells from both sites and analyzed gene expression of single cells. Aggregating all data points, we identified 14 cell clusters in an unbiased manner based on differentially expressed genes (Fig. 4 A). Strikingly, comparison of gingiva and BM HSCs on the 2D cluster projection demonstrated no major differences in the subpopulations present at either site (Fig. 4 B). Validating our single-cell RNA-seq approach, we noted a separation of cells with gene modules for either an erythrocyte or joint lymphoid-myeloid program (Fig. S3, A–D), as has been previously described for lineage-depleted cKit$^+$ cells in the BM (Giladi et al., 2018). Moreover, we also identified gene modules associated with the most naive HSC state (Giladi et al., 2018); cells with a high stem score also had a low proliferation score (Fig. 4, C and D). Expression of this naive HSC signature was found in gingival CD45$^+$Lin$^-$cKit$^+$ cells (Fig. 4, C and D), implying that early HSCs were supported in this tissue and that healthy gingiva is able to support a comprehensive HSPC network.

Having established that the cellular identities of the gingiva and BM HSPC niches were similar, we next ascertained whether stimuli important for establishing BM hematopoiesis were important for hematopoiesis in the gingiva. The presence of a commensal flora and IFNα/β signaling are both required for normal BM hematopoiesis (Balmer et al., 2014; Essers et al., 2009; Khosravi et al., 2014). Similar to what has been described in the BM, gingiva HSPCs were altered in germ-free animals and animals in which IFNα/β signals were lacking (*Ifnar1*$^{-/-}$ mice; Fig. 4, E and F). These data indicate that factors important for regulating BM HSPCs are also important for gingival HSPCs.

However, HSPCs are exquisitely responsive to inflammatory stimuli, being remodeled by inflammation to provide the immune effectors needed for an immune response (Baldridge et al., 2010; Griseri et al., 2012; Nagai et al., 2006; Saenz et al., 2010; Siracusa et al., 2013). Therefore, we next queried whether gingival and BM HSPCs would similarly respond to inflammatory stimuli. First, we induced inflammation local to the gingiva, using ligature-induced periodontitis (LIP) to drive oral inflammation (Abe and Hajishengallis, 2013). In response to local inflammation, gingiva HSPCs expanded (Fig. 4 G), resulting in increased hematopoietic activity in gingival tissue and therefore

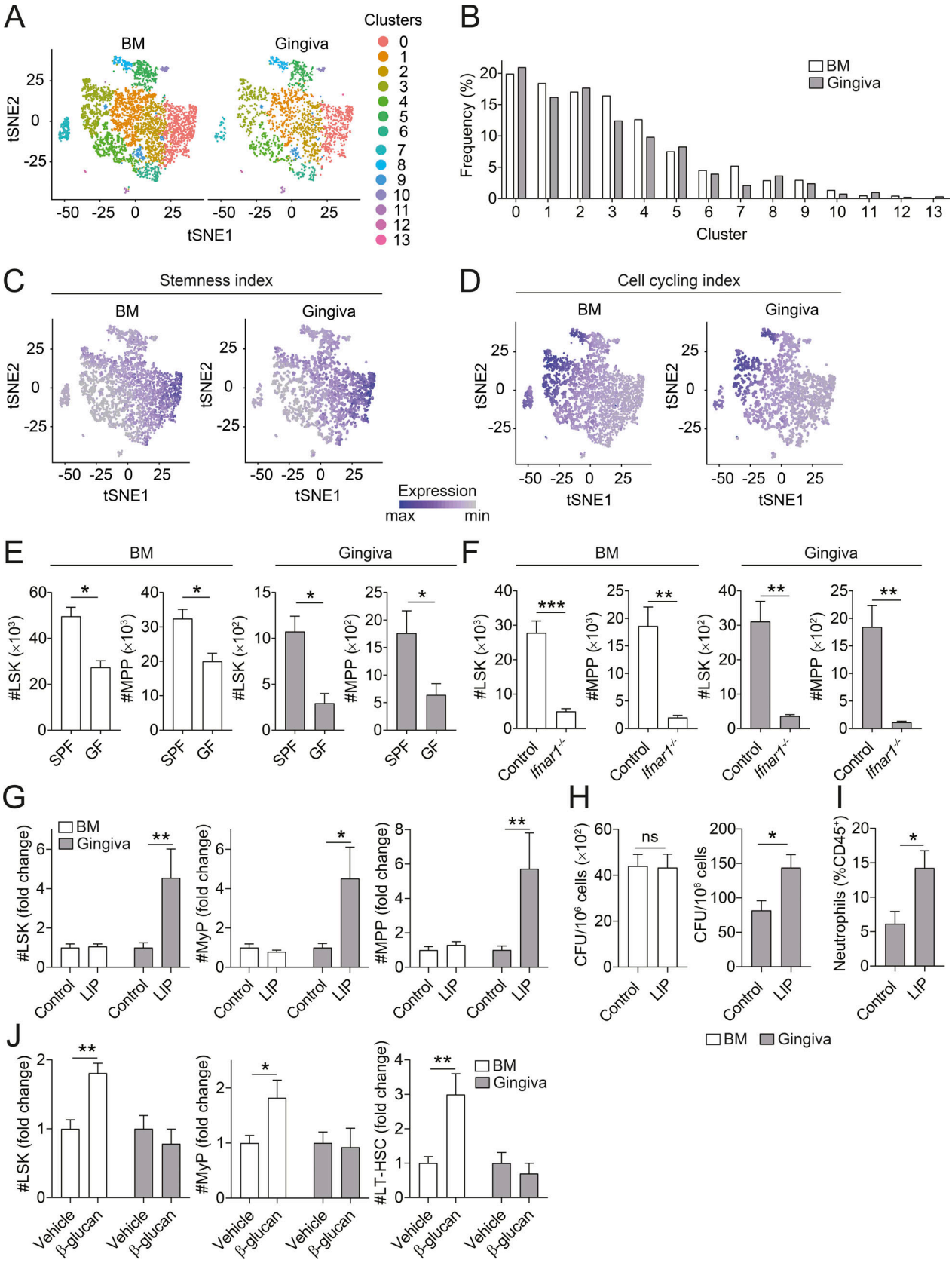

Figure 4. **BM and gingiva HSPCs exhibit distinct responsiveness to inflammation. (A–D)** Total LSK + MyP cells were isolated by FACS from the gingiva and BM of mice and analyzed by single-cell RNA-seq. **(A)** tSNE plots show clustering in the two tissues. **(B)** Bar graph showing frequencies of cells in each cluster in BM (white bars) and gingiva (gray bars) samples. **(C and D)** Projection of the stemness and cell cycling index scores (from Giladi et al., 2018) onto the core model to identify their distribution across the clusters in the BM and gingiva. **(E and F)** Number of LSKs and MPPs in the BM per femur and gingiva of

germ-free (GF) mice and specific pathogen–free (SPF) controls (E) or *Ifnar1*$^{-/-}$ and controls (F). n = 6–9 mice per group. **(G–I)** LIP was induced in cohorts of mice, and HSPCs in the gingiva and BM were examined 10 d after ligature placement. **(G)** Graph shows fold-change in the numbers of LSK, MyP, and MPP cells in the gingiva and BM. n = 6 mice per group pooled from two independent experiments. **(H)** CFU activity from MethoCult cultures of BM (left) and gingiva (right). n = 6 mice pooled from four independent experiments. **(I)** Neutrophil output in MethoCult cultures of gingiva and BM assessed by flow cytometry. n = 6 mice per group pooled from four independent experiments. **(J)** Fold-change in the numbers of LSK, MyP, and LT-HSCs in the gingiva and BM 7 d following i.p. administration of β-glucan. n = 5–7 mice per group pooled from three independent experiments. Data are presented as mean ± SEM. Statistical comparisons were performed using an unpaired t test (E and J) with Welch's correction (F, H, and I), a two-way ANOVA with a Holm–Šídák post hoc test (G). ***, P < 0.001; **, P < 0.01; *, P < 0.05.

increased CFU activity per cell in MethoCult assays (Fig. 4 H). Importantly, this HSPC remodeling driven by oral inflammation was gingiva specific, as no changes to HSPC populations were seen in the BM of LIP mice (Fig. 4, G and H). Focusing on the expanded HSPC network in the gingiva, we noted an altered differentiation potential, with increased production of neutrophils in Methocult assays of gingiva from LIP compared with controls (Fig. 4 I). To explore this altered differentiation potential further, we sorted LSK and MyP from LIP and control mice and cultured these cells in MethoCult medium. LSK from LIP mice exhibited increased CFU capacity and generated increased proportions of neutrophils (Fig. S3, E and F). Examining this in vivo, we transferred total HSPCs (i.e., LSK + MyP) from control or LIP mice, alongside total BM cells from a third congenically distinct donor, into irradiated recipients. When reconstitution was examined after 10 wk, HSPCs from LIP mice gave rise to increased proportions of neutrophils, although no increases in reconstitution capacity were seen (Fig. S3, G and H). Combined, these data outline clear alterations to the local, gingiva-resident HSPC network in response to oral inflammation; such alterations are specific to this site and not seen in BM HSPCs.

Next, we ascertained whether inflammatory stimuli shown to remodel the BM niche could impact gingival HSPCs. Recently, β-glucan has been shown to drive trained immunity through modulation of BM HSPCs and hematopoiesis (Mitroulis et al., 2017). We injected mice with β-glucan and saw the previously described increases in BM HSPC populations (Mitroulis et al., 2017; Fig. 4 J). These changes in BM HSPCs in response to β-glucan were tissue specific; gingival HSPCs were unchanged following β-glucan administration (Fig. 4 J). Exploring the impact of systemic inflammation on gingival hematopoiesis further, we injected mice with LPS, a stimulus shown to drive more substantial changes to BM HSPCs. LPS injection induced the previously reported expansion of LSK in the BM (Fig. S3 I; Scumpia et al., 2010). Again, this was not seen in the gingival HSPC compartment (Fig. S3 I). However, the gingival HSPC niche did exhibit decreases in MyP that were also seen in the BM HSPC niche (Fig. S3 J). Combined, these data highlight that healthy gingiva houses HSPCs that, in response to local inflammation, are remodeled to promote enhanced production of neutrophils. In contrast, our data demonstrate that in response to systemic inflammatory stimuli, the gingival HSPC niche responds differently from the BM niche. Indeed, gingiva HSPCs were protected from certain systemic inflammatory stimuli capable of altering output of innate cells from the BM.

Circulating HSPCs are retained within inflamed tissues (Massberg et al., 2007); sensitive to signals of tissue distress, HSPCs become tissue resident and undergo EMH to generate effector cells that contribute to the ongoing inflammatory response (Griseri et al., 2012; Saenz et al., 2010; Siracusa et al., 2013). In this way, EMH is a key mechanism of effective immunity. As such, at barrier sites, EMH has been shown to occur in response to pathogen challenge and injury (Fu et al., 2019; Kim et al., 2011; Saenz et al., 2010; Siracusa et al., 2013). Moreover, HSPCs resident in inflamed barriers have been shown to be mediators of the pathophysiological network driving disease in a number of settings (Griseri et al., 2012; Siracusa et al., 2013). Standing in contrast to these pivotal roles for extramedullary HSPCs in contributing to active inflammation, we demonstrate that HSPCs are present in healthy gingiva tissue. The HSPCs identified in gingival tissue were present in the absence of any current or past inflammatory challenge, in naive animals that had no history of inflammation. In health, few tissues support EMH; predominantly during development, but also later in life, the liver, spleen, and muscle can house HSPCs (Cardier and Barberá-Guillem, 1997; McKinney-Freeman et al., 2002; Morrison et al., 1997). Of particular interest, the lung has been shown to be a reservoir for megakaryocytes and HSPCs that are important for platelet generation (Lefrançais et al., 2017), and fetal skin can support megakaryocyte-erythroid-mast cell progenitors and erythropoiesis (Popescu et al., 2019). Distinct from this, we show local generation of multiple populations of short-lived myeloid cells at a healthy barrier site, which then constitute components of the local immune network. Moreover, we show that the gingiva houses naive HSCs, not just later progenitor stages that are supplied by the BM. These data highlight a unique mechanism of myeloid cell development and instruction at the gingiva. Our studies should now be extended to examine human gingiva, ascertaining the role of gingival hematopoiesis on human oral health.

What would be the biological necessity for the gingiva to support the local development of a proportion of myeloid cells? The gingiva exhibits a very high demand for innate cells at steady state, with large populations of both neutrophils and monocytes present. Indeed, there are much larger populations of monocytes and neutrophils in the gingiva than any other healthy barrier. Although we have not detailed the lifespans or ultimate fates of these populations in the gingiva, it could be hypothesized that generation of these short-lived innate immune mediators would ordinarily place a high demand on BM hematopoiesis, a process that must be strictly controlled to prevent BM HSC exhaustion. Relocating production of innate cells from the BM to the gingiva would reduce the stress placed on the BM niche and concomitantly safeguard the function of gingiva-generated innate cells from distal/systemic inflammatory signals. In addition

to this, locally generated innate cells could exhibit altered functions, exquisitely tailored to promote gingival health, a key future line of inquiry.

Combined, our data indicate that some myeloid cells, including monocytes and neutrophils, present in the gingiva develop locally from barrier-resident HSPCs. Together, our data outline a unique mechanism that enforces local control over the innate immune cells policing the gingival barrier, redefining our understanding of how innate immune cells develop and are instructed to appropriately function at this site.

Materials and methods

Mice

C57BL/6 were purchased from Envigo. *Ccr2*$^{-/-}$ (originally from The Jackson Laboratory), *Ifnar1*$^{-/-}$(Müller et al., 1994; provided by C. Reis e Sousa, The Francis Crick Institute, London, UK), congenic CD45.1 C57BL/6, and congenic CD45.1/CD45.2 C57BL/6 mice were bred in house. Germ-free mice and specific pathogen–free controls were obtained from the University of Manchester Axenic and Gnotobiotic Facility. All experiments were approved by the University of Manchester Animal Welfare Ethical Review Body and the Home Office, UK, and performed following local rules. All mice, except germ free, were housed under specific pathogen–free conditions, and all experiments used age- and sex-matched animals.

Generation of chimeras

For head-shielded chimeras, host mice were anesthetized by i.p. administration of ketamine (80 mg/kg; Vetoquinol) and xylazine (8 mg/kg; Bayer). Mice received either total-body irradiation or were irradiated with their heads positioned beneath lead shielding. In both cases, mice received a total of 11 Gy irradiation as a split dose. Mice were reconstituted by i.v. injection with 5–10 × 10^6 donor BM cells from congenic animals that had been depleted of CD90 cells by MACS microbeads (Miltenyi Biotec) according to the manufacturer's instructions. For experiments examining the differentiation potential of sorted HSPC populations, 200 or 500 FACS-purified CD45$^+$Lin$^-$cKit$^+$ cells were transferred alongside 4–5 × 10^6 congenic donor BM. Mice were maintained on 0.03% enrofloxacin (Bayer) supplied through drinking water 1 wk before and 4 wk after irradiation. After irradiation, mice were housed in autoclaved cages with sterile drinking water, food, bedding, and enrichment. Reconstitution was allowed to occur for a minimum of 8 wk before analysis.

LIP

Bone loss was induced through the use of a 5-0 silk ligature tied around the maxillary second molars, with the ligature placed in the gingival sulcus as previously described (Abe and Hajishengallis, 2013); this treatment induces bone loss, which was measured 10 d after ligature placement.

In vivo treatments

Mice were i.p. dosed with 1 mg of β-glucan (InvivoGen) dissolved in sterile water and euthanized 7 d after treatment to harvest tissues. For in vivo CD45 labeling experiments, mice received 1 µg anti–CD45-AF700 (BioLegend) i.v. and were euthanized 5 min after treatment. For EdU labeling experiments, mice were i.p. dosed with 0.5 mg EdU (Life Technologies) per mouse and euthanized 4 or 24 h after treatment. Mice were i.p. dosed with 5 µg LPS (*Escherichia coli* O111:B4; InvivoGen) and euthanized 18 h after treatment.

Preparation of single-cell suspensions

Gingiva

Mouse gingiva were dissected as previously described (Dutzan et al., 2016a). Briefly, tissue blocks were dissected and digested for 30 min at 37°C in RPMI 1640 (Sigma-Aldrich; henceforth called medium) supplemented with 2 mM L-glutamine (Sigma-Aldrich), 10 mM Hepes (Sigma-Aldrich), 3.2 mg/ml collagenase IV (Gibco), and 7.5 µg/ml DNase (Sigma-Aldrich). Following removal of gingiva tissue from maxilla and mandible, single-cell suspensions were obtained by mashing tissues through a 70-µm cell strainer.

Blood

Blood was harvested by cardiac puncture into medium containing 6.25 mM EDTA (Sigma-Aldrich) supplemented with 3% FCS. Red blood cells were lysed by incubation with ammonium-chloride-potassium lysing buffer (Lonza) for 3 min on ice twice.

BM

Single-cell suspensions were prepared from the BM by flushing the marrow out of femurs, followed by red blood cell lysis as described above.

Small intestine and colonic lamina propria

Cells were isolated as previously described (Shaw et al., 2018). Briefly, the small intestine and colon were rapidly dissected, Peyer's patches removed, longitudinally cut, and washed in PBS. Intestinal epithelial cells were removed by chopping tissues into 2–3-cm segments, which were incubated for 20 min at 37°C with vigorous agitation in medium containing 3% FCS, 20 mM Hepes, 100 U/ml polymyxin B (Sigma-Aldrich), 5 mM EDTA, and 1 mM freshly thawed dithiothreitol. After incubation, tissues were repeatedly shaken in fresh serum-free medium with 2 mM EDTA and 20 mM Hepes to further dissociate intestinal epithelial cells and leukocytes. The remaining lamina propria and muscularis were minced and digested (37°C, 30 min) with continuous stirring in serum-free medium with 20 mM Hepes, 0.1 mg/ml Liberase TL (Roche), and 0.5 mg/ml DNase. The tissue was mashed through a 70-µm cell strainer and subsequently a 40-µm cell strainer to obtain single-cell suspensions.

Skin

The dorsal and ventral sides of the ear were separated. This tissue was digested in medium with 0.25 mg/ml Liberase TL and 0.5 mg/ml DNase for 105 min at 37°C. The reaction was stopped with 0.5 M EDTA, and the tissue was processed with a Medi-Machine (BD Biosciences) system for 6 min. Cell suspensions from Medicons were washed with 8 ml complete medium with 0.5 mg/ml DNase and passed through a 100-µm strainer to obtain a single-cell suspension.

Spleen and submandibular lymph nodes

Spleens and lymph nodes were mashed through a 70-µm strainer. For spleens, red blood cells were lysed as described above.

Lung

Lungs were finely minced and incubated in medium with 0.1 mg/ml Liberase TL and 0.25 mg/ml DNase for 20 min at 37°C in a shaking incubator. Cells were mashed through a 70-µm cell strainer, and red blood cells were lysed and washed to obtain a single-cell suspension.

Flow cytometry

Single-cell suspensions from tissues were washed in PBS and incubated with antibody cocktails in FACS buffer (PBS with 2% FCS and 2 mM EDTA) or PBS with anti-CD16/32 (2.4G2; BioXcell) for 15 min at 4°C. Dead cells were excluded by use of a Live/Dead Fixable blue dead cell stain kit (Molecular Probes), Zombie UV, or Aqua Fixable Viability Kit (BioLegend). When biotin-conjugated antibodies were used, cells were washed and stained with fluorochrome-conjugated streptavidin (BioLegend) for 10 min at 4°C. Cells were fixed in 2% paraformaldehyde (Sigma-Aldrich) for 10 min at room temperature, washed, and finally resuspended in PBS before acquisition. EdU staining was performed after fixation using Click-iT EdU Cell Proliferation Kit (Thermo Fisher Scientific) according to the manufacturer's instructions. Cell were stained with combinations of the following antibodies, which were obtained from eBioscience, BD PharMingen, and BioLegend: CD45 (30-F11), CD45.1 (A20), CD45.2 (104), CD3ε (145-2C11), TCR-β (H57-597), CD19 (1D3), B220 (RA3-6B2), Ly6G (1A8), NK1.1 (PK136), Ter119 (TER-119), Siglec F (E50-2440), FcεR1α (MAR-1), CD49b (HMα2), CD11b (M1/70), Ly6C (HK1.4), CD64 (X54-5/7.1), F4/80 (BM8), CX3CR1 (SA011F11), CD44 (IM7), CCR2 (SA203G11), CD68 (FA-11), I-A/I-E (M5/114.15.2), CD11c (N418), Sca-1 (D7), cKit (2B8), CD150 (TC15-12F12.2), CD48 (HM48-1), Flt3 (A2F10), CD34 (RAM34), CD16/32 (93), CD101 (Moushi101), CXCR4 (L276F12), CD27 (LG.3A10), and CD201 (1560). Samples were acquired using a BD LSRFortessa or FACSymphony (BD Biosciences) flow cytometer and analyzed with FlowJo software (TreeStar). Where appropriate, dimensional reduction was performed using the t-distributed stochastic neighbor embedding (tSNE) algorithm in FlowJo.

Monocytes were identified as $CD45^+Lin^-$ (CD3ε, TCR-β, CD19, B220, NK1.1, Ter119, Siglec F, and Ly6G) $CD11b^+Ly6C^{hi}CD64^-MHCII^-$. HSPCs were identified as follows: LSK, $CD45^+Lin^-$ (CD3ε, TCR-β, CD19, B220, NK1.1, Ter119, Siglec F, Ly6G, FcεR1α, CD11b, CD11c, and Ly6C) $Sca\text{-}1^+cKit^+$; MyP, $CD45^+Lin^-Sca\text{-}1^-cKit^+$; long-term HSC, LSK $CD150^+CD48^-$; short-term HSC, LSK $CD150^-CD48^-$; MPP, LSK $CD150^-CD48^+$; MPP4, LSK $Flt3^+CD48^+$; granulocyte-monocyte progenitor, MyP $CD16/32^{hi}CD34^+$; and CMP, MyP $CD16/32^{int}CD34^+$.

Monocyte and HSPC isolation by FACS

Single-cell suspensions of blood, BM, gingiva, skin, and the small intestine were prepared as previously described and suspended in FACS buffer. Cells were sorted using a BD FACSAria Fusion (BD Biosciences). Monocytes were sorted using the same gating as in Fig. S1 A, and HSPCs were sorted using the strategy outlined in Fig. 2 A. For cytospins, MethoCult, chimera experiments, and macrophage differentiation cultures, cells were collected in complete RPMI with 10% FCS. For bulk RNA-seq experiments, cells were collected in RLT buffer (Qiagen) containing β-mercaptoethanol. Cells were collected in 50% RPMI/50% FCS for single-cell sequencing experiments.

M-CSF macrophage-monocyte cultures

Monocytes sorted from the gingiva or BM were cultured for 7 d in 96-well round-bottom plates (Corning) in RPMI 1640 supplemented with 10 mM Hepes, 100 U/ml penicillin, 100 µg/ml streptomycin, 2 mM L-glutamine, MEM nonessential amino acids, 10% FCS, and 20 ng/ml M-CSF (Peprotech). Cells were washed with PBS and detached using Accutase (StemCell Technologies) according to the manufacturer's instructions and were analyzed by flow cytometry.

Bulk RNA-seq

Total RNA from ∼700–40,000 FACS-sorted monocytes was isolated using the Single Cell RNA Purification Kit (Norgen Biotek Corp.) according to the manufacturer's instructions. RNA samples were precipitated adding 0.1 volume of 3 M sodium acetate and 2 volumes of 100% ethanol and shipped on dry ice to Theragen Etex Bio (South Korea) for sequencing. Briefly, cDNA libraries were generated using the SMART-Seq V3 Ultra Low Input RNA Kit (CloneTech), and samples were sequenced on the Illumina HiSeq2500PE sequencing platform. Reads were filtered with Trimmomatic (v0.36). Filtered fastq files were aligned to the GENCODE genome (GRCm38.p5) using STAR (v2.5.3). Filtered reads were then sorted, compressed, and unaligned reads removed using samtools (v0.1.18). Aligned reads were then counted, normalized, and compared using the Cuffquant, Cuffnorm, and Cuffdiff functions, respectively, of Cufflinks (v2.2.1). Genes were clustered using Morpheus (Broad Institute, https://software.broadinstitute.org/morpheus/). The enrichment of gene ontology terms was determined using Panther. ArrayExpress accession no. E-MTAB-10039.

Single-cell RNA-seq

Single-cell isolation and library construction

Single-cell suspensions of gingival and BM HSPCs were FACS purified. Gene expression libraries were prepared from single cells using the Chromium Controller and Single Cell 3′ Reagent Kit v3 (10x Genomics) according to the manufacturer's protocol. Briefly, nanoliter-scale gel beads in emulsion (GEMs) were generated by combining barcoded gel beads, a master mix containing cells, and partitioning oil onto a chromium chip. Cells were delivered at a limiting dilution, such that the majority (90–99%) of generated GEMs contain no cells, while the remainder largely contain a single cell. The Gel Beads were then dissolved, primers were released, and any copartitioned cells were lysed. Primers containing an Illumina TruSeq Read 1 sequencing primer, a 16-nt 10x Barcode, a 12-nt unique molecular identifier, and a 30-nt poly(dT) sequence were then mixed with the cell lysate and a master mix containing reverse transcription reagents. Incubation of the GEMs then yielded barcoded cDNA

from polyadenylated mRNA. Following incubation, GEMs were broken, and pooled fractions were recovered. First-strand cDNA was then purified from the post-GEM–reverse transcription reaction mixture using silane magnetic beads and amplified via PCR to generate sufficient mass for library construction. Enzymatic fragmentation and size selection were then used to optimize the cDNA amplicon size. Illumina P5 and P7 sequences, a sample index, and TruSeq Read 2 sequence were added via end repair, A-tailing, adaptor ligation, and PCR to yield final Illumina-compatible sequencing libraries.

Sequencing

The resulting sequencing libraries comprised standard Illumina paired-end constructs flanked with P5 and P7 sequences. The 16-bp 10x Barcode and 12-bp unique molecular identifier were encoded in Read 1, while Read 2 was used to sequence the cDNA fragment. Sample index sequences were incorporated as the i7 index read. Paired-end sequencing (28:98) was performed on the Illumina NextSeq500 platform using NextSeq 500/550 High Output v2.5 (150 Cycles) reagents. The .bcl sequence data were processed for quality control purposes using bcl2fastq software (v2.20.0.422), and the resulting .fastq files were assessed using FastQC (v0.11.3), FastqScreen (v0.9.2), and FastqStrand (v0.0.5) before preprocessing with the CellRanger pipeline.

Data processing

Cells with >10% mitochondrial reads were filtered out. The remaining cells were normalized, integrated (using IntegrateData), and analyzed with Seurat (v3.0). Module enrichment is presented as the transcript count of the genes comprising the cell module over the total transcript count of each cell and visualized using FeaturePlot (Seurat v3.0). On average, 3,360 genes for the gingiva and 3,096 genes for the BM were detected per cell. ArrayExpress accession no. E-MTAB-10050.

MethoCult assays

Total cell preparations from tissues or flow cytometry–purified HSPC populations were suspended in methylcellulose medium to quantify clonogenic CFUs (MethoCult GF M3434; StemCell Technologies). Cultures were incubated at 37°C with 5% CO_2 for 9–10 d before colonies were assessed and counted using an inverted microscope. Images of colonies were taken at 4×/UPlanFL N objective on the bright-field setting of an Olympus MMI Cell Cut Laser Microdissection System and white balanced using MMI CellTools software.

Cytospin

Monocytes and macrophages FACS purified from the gingiva were mounted on Superfrost slides (Thermo Fisher Scientific) using a Cytospin centrifuge (Cytospin 4; Thermo Fisher Scientific). Cells were fixed with ice-cold methanol and stored at room temperature before staining with hematoxylin and acidic eosin (Thermo Fisher Scientific) and mounted with DPX (Thermo Fisher Scientific). Images were captured using an Olympus BX63 upright microscope. Images were then processed and analyzed using Fiji ImageJ.

Immunofluorescent imaging

Gingiva was fixed for 24 h in 4% paraformaldehyde (Sigma-Aldrich) before decalcification in Osteosoft (Merck Millipore) and storage in 70% ethanol until processing. Paraffin-embedded sections were deparaffinized and rehydrated. Antigen retrieval was performed through incubation with trypsin (1 mg/ml; for Ly6G) or proteinase K (20 µg/ml; for F4/80 and Ly6C) for 15 min at 37°C. Avidin biotin blocking was performed as per the manufacturer's instructions (BioLegend) before incubation with primary antibodies against Ly6C (0.7 mg/ml; Abcam), Ly6G (0.32 mg/ml; Abcam), and F4/80 (0.5 mg/ml; Invitrogen) overnight at 4°C. Sections were incubated with appropriate biotinylated secondary antibodies before performing tyramide AF555 amplification as per the manufacturer's instructions (Invitrogen). Sections were counterstained with DAPI (1 µg/ml) and mounted. Images were collected at room temperature on a Zeiss Axioimager.D2 upright microscope using either a 5×/0.16 EC Plan-neofluar or 10×/0.3 EC Plan-neofluar objective and captured using a Photometrics Coolsnap HQ2 camera through Micromanager software v1.4.23. Images were processed with Fiji Image J v2.1.0/1.53c following acquisition.

Statistics

Statistical analyses were performed using GraphPad Prism 7/8, and data are presented as mean ± SEM in all cases unless otherwise indicated. Statistical testing between two groups was performed using a Student's *t* test for paired experimental data, an unpaired *t* test with Welch's correction, or a Mann–Whitney *U* test. When comparing more than two groups, a one-way ANOVA or a two-way ANOVA with appropriate post hoc tests was used.

Online supplemental material

Fig. S1 shows that a unique monocyte population is present in the gingiva. Fig. S2 shows that HSPCs are present in gingiva tissue and exhibit hematopoietic activity. Fig. S3 details how HSPCs in the gingiva and BM exhibit altered responsiveness to inflammatory signals.

Acknowledgments

We thank Dr T. Zangerle-Murray for technical support and Profs. J. Allen, R. Grencis, and M. Travis and Dr. M. Hepworth for critical review of our manuscript. Theragen Etex Bio Institute (Republic of Korea) rendered sequencing services for samples used in this study.

This study was funded by the Biotechnology and Biological Sciences Research Council (BB/M025977/1 to J.E. Konkel and BB/S01130X/1 to T.N. Shaw), the Lister Institute (Prize Fellowship to J.E. Konkel), and Versus Arthritis (awarded to J.E. Konkel and F.A. McClure). J.R. Grainger is supported by a Kennedy Trust for Rheumatology Research Senior Fellowship. The University of Manchester Axenic and Gnotobiotic facility used was established with the support of the Wellcome Trust (097820/Z/11/B). We acknowledge the support of the Bioimaging, Flow Cytometry, Genomic Technologies, Bioinformatics and Biological Services core facilities at the University of Manchester.

Author contributions: J.E. Konkel and J.R. Grainger conceived of and designed the experiments; J.E. Konkel., S. Krishnan, F.A. McClure, C. O'Boyle, K. Wemyss, T.N. Shaw, and H. Bridgeman performed the experiments; J.E. Konkel., S. Krishnan, C. O'Boyle, K. Wemyss, T.N. Shaw, and I.E. Prise analyzed and interpreted the data; J.E. Konkel and S. Krishnan wrote, reviewed, and edited the paper. All authors provided final approval and vouched for the content of the final manuscript.

Disclosures: The authors declare no competing interests exist.

Submitted: 17 April 2020
Revised: 3 December 2020
Accepted: 29 January 2021

References

Abe, T., and G. Hajishengallis. 2013. Optimization of the ligature-induced periodontitis model in mice. *J. Immunol. Methods.* 394:49–54. https://doi.org/10.1016/j.jim.2013.05.002

Anderson, K.G., K. Mayer-Barber, H. Sung, L. Beura, B.R. James, J.J. Taylor, L. Qunaj, T.S. Griffith, V. Vezys, D.L. Barber, and D. Masopust. 2014. Intravascular staining for discrimination of vascular and tissue leukocytes. *Nat. Protoc.* 9:209–222. https://doi.org/10.1038/nprot.2014.005

Atarashi, K., W. Suda, C. Luo, T. Kawaguchi, I. Motoo, S. Narushima, Y. Kiguchi, K. Yasuma, E. Watanabe, T. Tanoue, et al. 2017. Ectopic colonization of oral bacteria in the intestine drives T_H1 cell induction and inflammation. *Science.* 358:359–365. https://doi.org/10.1126/science.aan4526

Bain, C.C., C.L. Scott, H. Uronen-Hansson, S. Gudjonsson, O. Jansson, O. Grip, M. Guilliams, B. Malissen, W.W. Agace, and A.M. Mowat. 2013. Resident and pro-inflammatory macrophages in the colon represent alternative context-dependent fates of the same Ly6Chi monocyte precursors. *Mucosal Immunol.* 6:498–510. https://doi.org/10.1038/mi.2012.89

Baldridge, M.T., K.Y. King, N.C. Boles, D.C. Weksberg, and M.A. Goodell. 2010. Quiescent haematopoietic stem cells are activated by IFN-gamma in response to chronic infection. *Nature.* 465:793–797. https://doi.org/10.1038/nature09135

Balmer, M.L., C.M. Schürch, Y. Saito, M.B. Geuking, H. Li, M. Cuenca, L.V. Kovtonyuk, K.D. McCoy, S. Hapfelmeier, A.F. Ochsenbein, et al. 2014. Microbiota-derived compounds drive steady-state granulopoiesis via MyD88/TICAM signaling. *J. Immunol.* 193:5273–5283. https://doi.org/10.4049/jimmunol.1400762

Cardier, J.E., and E. Barberá-Guillem. 1997. Extramedullary hematopoiesis in the adult mouse liver is associated with specific hepatic sinusoidal endothelial cells. *Hepatology.* 26:165–175. https://doi.org/10.1002/hep.510260122

Chong, S.Z., M. Evrard, S. Devi, J. Chen, J.Y. Lim, P. See, Y. Zhang, J.M. Adrover, B. Lee, L. Tan, et al. 2016. CXCR4 identifies transitional bone marrow premonocytes that replenish the mature monocyte pool for peripheral responses. *J. Exp. Med.* 213:2293–2314. https://doi.org/10.1084/jem.20160800

Dutzan, N., L. Abusleme, H. Bridgeman, T. Greenwell-Wild, T. Zangerle-Murray, M.E. Fife, N. Bouladoux, H. Linley, L. Brenchley, K. Wemyss, et al. 2017. On-going Mechanical Damage from Mastication Drives Homeostatic Th17 Cell Responses at the Oral Barrier. *Immunity.* 46:133–147. https://doi.org/10.1016/j.immuni.2016.12.010

Dutzan, N., L. Abusleme, J.E. Konkel, and N.M. Moutsopoulos. 2016a. Isolation, Characterization and Functional Examination of the Gingival Immune Cell Network. *J. Vis. Exp.* (108):e53736. https://doi.org/10.3791/53736

Dutzan, N., J.E. Konkel, T. Greenwell-Wild, and N.M. Moutsopoulos. 2016b. Characterization of the human immune cell network at the gingival barrier. *Mucosal Immunol.* 9:1163–1172. https://doi.org/10.1038/mi.2015.136

Essers, M.A., S. Offner, W.E. Blanco-Bose, Z. Waibler, U. Kalinke, M.A. Duchosal, and A. Trumpp. 2009. IFNalpha activates dormant haematopoietic stem cells in vivo. *Nature.* 458:904–908. https://doi.org/10.1038/nature07815

Evrard, M., I.W.H. Kwok, S.Z. Chong, K.W.W. Teng, E. Becht, J. Chen, J.L. Sieow, H.L. Penny, G.C. Ching, S. Devi, et al. 2018. Developmental Analysis of Bone Marrow Neutrophils Reveals Populations Specialized in Expansion, Trafficking, and Effector Functions. *Immunity.* 48:364–379.e8. https://doi.org/10.1016/j.immuni.2018.02.002

Fu, J., J. Zuber, M. Martinez, B. Shonts, A. Obradovic, H. Wang, S.P. Lau, A. Xia, E.E. Waffarn, K. Frangaj, et al. 2019. Human Intestinal Allografts Contain Functional Hematopoietic Stem and Progenitor Cells that Are Maintained by a Circulating Pool. *Cell Stem Cell.* 24:227–239.e8. https://doi.org/10.1016/j.stem.2018.11.007

Giladi, A., F. Paul, Y. Herzog, Y. Lubling, A. Weiner, I. Yofe, D. Jaitin, N. Cabezas-Wallscheid, R. Dress, F. Ginhoux, et al. 2018. Single-cell characterization of haematopoietic progenitors and their trajectories in homeostasis and perturbed haematopoiesis. *Nat. Cell Biol.* 20:836–846. https://doi.org/10.1038/s41556-018-0121-4

Ginhoux, F., and S. Jung. 2014. Monocytes and macrophages: developmental pathways and tissue homeostasis. *Nat. Rev. Immunol.* 14:392–404. https://doi.org/10.1038/nri3671

Granick, J.L., S.I. Simon, and D.L. Borjesson. 2012. Hematopoietic stem and progenitor cells as effectors in innate immunity. *Bone Marrow Res.* 2012:165107. https://doi.org/10.1155/2012/165107

Griseri, T., B.S. McKenzie, C. Schiering, and F. Powrie. 2012. Dysregulated hematopoietic stem and progenitor cell activity promotes interleukin-23-driven chronic intestinal inflammation. *Immunity.* 37:1116–1129. https://doi.org/10.1016/j.immuni.2012.08.025

Guilliams, M., A. Mildner, and S. Yona. 2018. Developmental and Functional Heterogeneity of Monocytes. *Immunity.* 49:595–613. https://doi.org/10.1016/j.immuni.2018.10.005

Hettinger, J., D.M. Richards, J. Hansson, M.M. Barra, A.C. Joschko, J. Krijgsveld, and M. Feuerer. 2013. Origin of monocytes and macrophages in a committed progenitor. *Nat. Immunol.* 14:821–830. https://doi.org/10.1038/ni.2638

Ingersoll, M.A., R. Spanbroek, C. Lottaz, E.L. Gautier, M. Frankenberger, R. Hoffmann, R. Lang, M. Haniffa, M. Collin, F. Tacke, et al. 2010. Comparison of gene expression profiles between human and mouse monocyte subsets. *Blood.* 115:e10–e19. https://doi.org/10.1182/blood-2009-07-235028

Khosravi, A., A. Yáñez, J.G. Price, A. Chow, M. Merad, H.S. Goodridge, and S.K. Mazmanian. 2014. Gut microbiota promote hematopoiesis to control bacterial infection. *Cell Host Microbe.* 15:374–381. https://doi.org/10.1016/j.chom.2014.02.006

Kim, M.H., J.L. Granick, C. Kwok, N.J. Walker, D.L. Borjesson, F.R. Curry, L.S. Miller, and S.I. Simon. 2011. Neutrophil survival and c-kit(+)-progenitor proliferation in Staphylococcus aureus-infected skin wounds promote resolution. *Blood.* 117:3343–3352. https://doi.org/10.1182/blood-2010-07-296970

Konkel, J.E., C. O'Boyle, and S. Krishnan. 2019. Distal Consequences of Oral Inflammation. *Front. Immunol.* 10:1403. https://doi.org/10.3389/fimmu.2019.01403

Kostic, A.D., D. Gevers, C.S. Pedamallu, M. Michaud, F. Duke, A.M. Earl, A.I. Ojesina, J. Jung, A.J. Bass, J. Tabernero, et al. 2012. Genomic analysis identifies association of Fusobacterium with colorectal carcinoma. *Genome Res.* 22:292–298. https://doi.org/10.1101/gr.126573.111

Krishnan, S., I.E. Prise, K. Wemyss, L.P. Schenck, H.M. Bridgeman, F.A. McClure, T. Zangerle-Murray, C. O'Boyle, T.A. Barbera, F. Mahmood, et al. 2018. Amphiregulin-producing γδ T cells are vital for safeguarding oral barrier immune homeostasis. *Proc. Natl. Acad. Sci. USA.* 115:10738–10743. https://doi.org/10.1073/pnas.1802320115

Lavin, Y., D. Winter, R. Blecher-Gonen, E. David, H. Keren-Shaul, M. Merad, S. Jung, and I. Amit. 2014. Tissue-resident macrophage enhancer landscapes are shaped by the local microenvironment. *Cell.* 159:1312–1326. https://doi.org/10.1016/j.cell.2014.11.018

Lefrançais, E., G. Ortiz-Muñoz, A. Caudrillier, B. Mallavia, F. Liu, D.M. Sayah, E.E. Thornton, M.B. Headley, T. David, S.R. Coughlin, et al. 2017. The lung is a site of platelet biogenesis and a reservoir for haematopoietic progenitors. *Nature.* 544:105–109. https://doi.org/10.1038/nature21706

Massberg, S., P. Schaerli, I. Knezevic-Maramica, M. Köllnberger, N. Tubo, E.A. Moseman, I.V. Huff, T. Junt, A.J. Wagers, I.B. Mazo, and U.H. von Andrian. 2007. Immunosurveillance by hematopoietic progenitor cells trafficking through blood, lymph, and peripheral tissues. *Cell.* 131:994–1008. https://doi.org/10.1016/j.cell.2007.09.047

McKinney-Freeman, S.L., K.A. Jackson, F.D. Camargo, G. Ferrari, F. Mavilio, and M.A. Goodell. 2002. Muscle-derived hematopoietic stem cells are hematopoietic in origin. *Proc. Natl. Acad. Sci. USA.* 99:1341–1346. https://doi.org/10.1073/pnas.032438799

Mildner, A., J. Schönheit, A. Giladi, E. David, D. Lara-Astiaso, E. Lorenzo-Vivas, F. Paul, L. Chappell-Maor, J. Priller, A. Leutz, et al. 2017. Genomic Characterization of Murine Monocytes Reveals C/EBPβ Transcription

Factor Dependence of Ly6C- Cells. *Immunity*. 46:849–862.e7. https://doi.org/10.1016/j.immuni.2017.04.018

Mitroulis, I., L.S. Chen, R.P. Singh, I. Kourtzelis, M. Economopoulou, T. Kajikawa, M. Troullinaki, A. Ziogas, K. Ruppova, K. Hosur, et al. 2017. Secreted protein Del-1 regulates myelopoiesis in the hematopoietic stem cell niche. *J. Clin. Invest.* 127:3624–3639. https://doi.org/10.1172/JCI92571

Morrison, S.J., D.E. Wright, and I.L. Weissman. 1997. Cyclophosphamide/granulocyte colony-stimulating factor induces hematopoietic stem cells to proliferate prior to mobilization. *Proc. Natl. Acad. Sci. USA.* 94: 1908–1913. https://doi.org/10.1073/pnas.94.5.1908

Moutsopoulos, N.M., and J.E. Konkel. 2018. Tissue-Specific Immunity at the Oral Mucosal Barrier. *Trends Immunol.* 39:276–287. https://doi.org/10.1016/j.it.2017.08.005

Müller, U., U. Steinhoff, L.F. Reis, S. Hemmi, J. Pavlovic, R.M. Zinkernagel, and M. Aguet. 1994. Functional role of type I and type II interferons in antiviral defense. *Science.* 264:1918–1921. https://doi.org/10.1126/science.8009221

Nagai, Y., K.P. Garrett, S. Ohta, U. Bahrun, T. Kouro, S. Akira, K. Takatsu, and P.W. Kincade. 2006. Toll-like receptors on hematopoietic progenitor cells stimulate innate immune system replenishment. *Immunity.* 24: 801–812. https://doi.org/10.1016/j.immuni.2006.04.008

Popescu, D.M., R.A. Botting, E. Stephenson, K. Green, S. Webb, L. Jardine, E.F. Calderbank, K. Polanski, I. Goh, M. Efremova, et al. 2019. Decoding human fetal liver haematopoiesis. *Nature.* 574:365–371. https://doi.org/10.1038/s41586-019-1652-y

Saenz, S.A., M.C. Siracusa, J.G. Perrigoue, S.P. Spencer, J.F. Urban Jr., J.E. Tocker, A.L. Budelsky, M.A. Kleinschek, R.A. Kastelein, T. Kambayashi, et al. 2010. IL25 elicits a multipotent progenitor cell population that promotes T(H)2 cytokine responses. *Nature.* 464:1362–1366. https://doi.org/10.1038/nature08901

Schiött, C.R., and H. Löe. 1970. The origin and variation in number of leukocytes in the human saliva. *J. Periodontal Res.* 5:36–41. https://doi.org/10.1111/j.1600-0765.1970.tb01835.x

Scumpia, P.O., K.M. Kelly-Scumpia, M.J. Delano, J.S. Weinstein, A.G. Cuenca, S. Al-Quran, I. Bovio, S. Akira, Y. Kumagai, and L.L. Moldawer. 2010. Cutting edge: bacterial infection induces hematopoietic stem and progenitor cell expansion in the absence of TLR signaling. *J. Immunol.* 184: 2247–2251. https://doi.org/10.4049/jimmunol.0903652

Serbina, N.V., and E.G. Pamer. 2006. Monocyte emigration from bone marrow during bacterial infection requires signals mediated by chemokine receptor CCR2. *Nat. Immunol.* 7:311–317. https://doi.org/10.1038/ni1309

Shaw, T.N., S.A. Houston, K. Wemyss, H.M. Bridgeman, T.A. Barbera, T. Zangerle-Murray, P. Strangward, A.J.L. Ridley, P. Wang, S. Tamoutounour, et al. 2018. Tissue-resident macrophages in the intestine are long lived and defined by Tim-4 and CD4 expression. *J. Exp. Med.* 215: 1507–1518. https://doi.org/10.1084/jem.20180019

Siracusa, M.C., S.A. Saenz, E.D. Wojno, B.S. Kim, L.C. Osborne, C.G. Ziegler, A.J. Benitez, K.R. Ruymann, D.L. Farber, P.M. Sleiman, et al. 2013. Thymic stromal lymphopoietin-mediated extramedullary hematopoiesis promotes allergic inflammation. *Immunity.* 39:1158–1170. https://doi.org/10.1016/j.immuni.2013.09.016

Tamoutounour, S., M. Guilliams, F. Montanana Sanchis, H. Liu, D. Terhorst, C. Malosse, E. Pollet, L. Ardouin, H. Luche, C. Sanchez, et al. 2013. Origins and functional specialization of macrophages and of conventional and monocyte-derived dendritic cells in mouse skin. *Immunity.* 39:925–938. https://doi.org/10.1016/j.immuni.2013.10.004

White, D.A., G. Tsakos, N.B. Pitts, E. Fuller, G.V. Douglas, J.J. Murray, and J.G. Steele. 2012. Adult Dental Health Survey 2009: common oral health conditions and their impact on the population. *Br. Dent. J.* 213:567–572. https://doi.org/10.1038/sj.bdj.2012.1088

JEM

Supplemental material

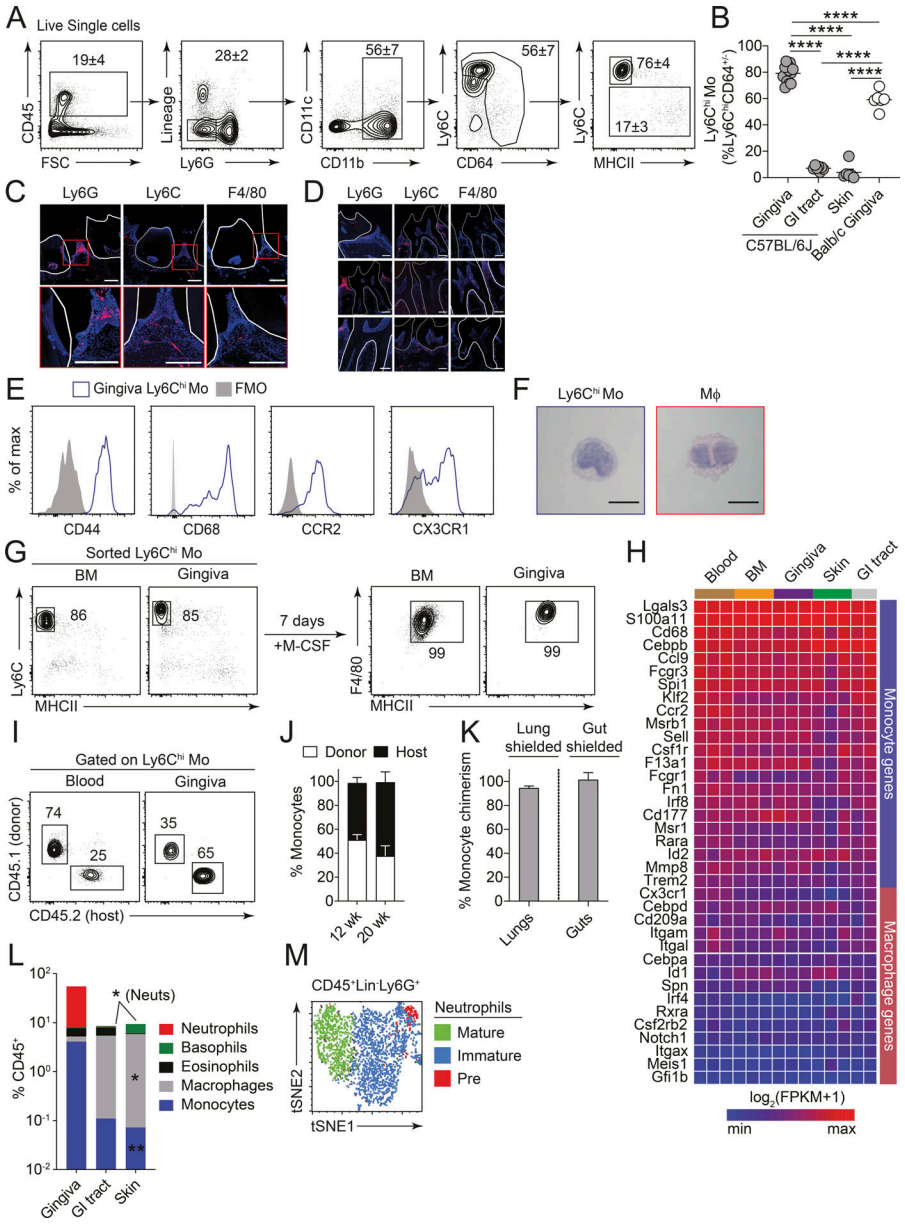

Figure S1. **A unique monocyte population is present in the gingiva. (A)** Gating strategy to identify monocytes in the gingiva and GI tract (numbers indicate frequencies expressed as mean ± SEM). **(B)** Quantification of monocytes as a percentage of live CD45$^+$Lin$^-$CD11b$^+$Ly6C$^{+/-}$CD64$^{+/-}$ cells (excludes Ly6C$^-$CD64$^-$ cells) in the gingiva of C57BL/6 and Balb/c mice and GI tract and skin of C57BL/6 mice. *n* = 6–13 mice per group. Lin = CD3ε, TCR-β, CD19, B220, NK1.1, Ter119, Siglec F, and Ly6G. **(C and D)** Representative staining of gingiva tissue for Ly6G$^+$, Ly6C^{bright}, and F4/80$^+$ cells. **(C)** Images show locations of cells staining positive for each marker. **(D)** Representative sections stained for Ly6G, Ly6C, and F4/80. Solid white line indicates edge of tooth. Scale bar = 200 µm. Staining from three separate experiments with *n* = 2–3 per experiment. **(E)** Representative histograms showing staining for CD44, CD68, CCR2, and CX3CR1 by gingival Ly6C^{hi} monocytes (Mo). Data from seven experiments with two to three mice per experiment. FMO, fluorescence minus one. **(F)** Cytospins of sorted gingival Ly6C^{hi} monocytes and macrophages (Mϕ) stained with H&E. Scale bar = 10 µm. Images are representative of two independent experiments. **(G)** Representative FACS plots of sorted BM and gingiva monocytes that were cultured with M-CSF for 7 d and analyzed by FACS. Data from two independent experiments. **(H)** Monocytes were FACS purified from the blood, BM, gingiva, skin, and GI tract and analyzed by RNA-seq. *n* = 2–3 biological replicates per group. Heatmap of the expression profile of canonical monocyte and macrophage-associated genes. FPKM, fragments per kilobase per million mapped reads. **(I)** Representative FACS plots showing host- and donor-derived Ly6C^{hi} monocytes in the blood and gingiva of head-shielded chimeras 20 wk after reconstitution. Numbers indicate percentage of cells in the gate. **(J)** Quantification of donor-derived (white bar) and host-derived (black bar) Ly6C^{hi} gingival monocytes 12 and 20 wk after reconstitution in head-shielded chimeras. *n* = 6–11 mice per group from two to three experiments. **(K)** Chimerism of Ly6C^{hi} monocytes in the lungs of torso-shielded chimeras (left) and GI tract of abdomen-shielded chimeras (right). The frequency of donor-derived Ly6C^{hi} gingiva monocytes was normalized to that of blood Ly6C^{hi} monocytes to determine percent chimerism. Data from one to two experiments with *n* = 3–9 mice per group. **(L)** Proportions of innate cells presented as the percentage of all CD45$^+$ cells in the gingiva, GI tract, and skin. *n* = 3 from three independent experiments. Asterisks indicate significant differences compared with gingiva. **(M)** tSNE map of CD45$^+$Lin$^-$Ly6G$^+$ gingival cells that were subjected to dimensional reduction based on Sca-1, cKit, CXCR2, CD45, Ly6G, CXCR4, MHCII, CD11b, Ly6C, CD11c, CD101, and Lin. Identified subpopulations are highlighted in the tSNE plot. Data representative of two experiments with *n* = 2–3 mice. Data are presented as mean ± SEM. Statistical comparisons were performed using a one-way ANOVA with a post hoc Tukey's test (B) and a two-way ANOVA with a Tukey's (L) and Holm–Šídák post hoc test (J); ****, P < 0.0001; **, P < 0.01; *, P < 0.05.

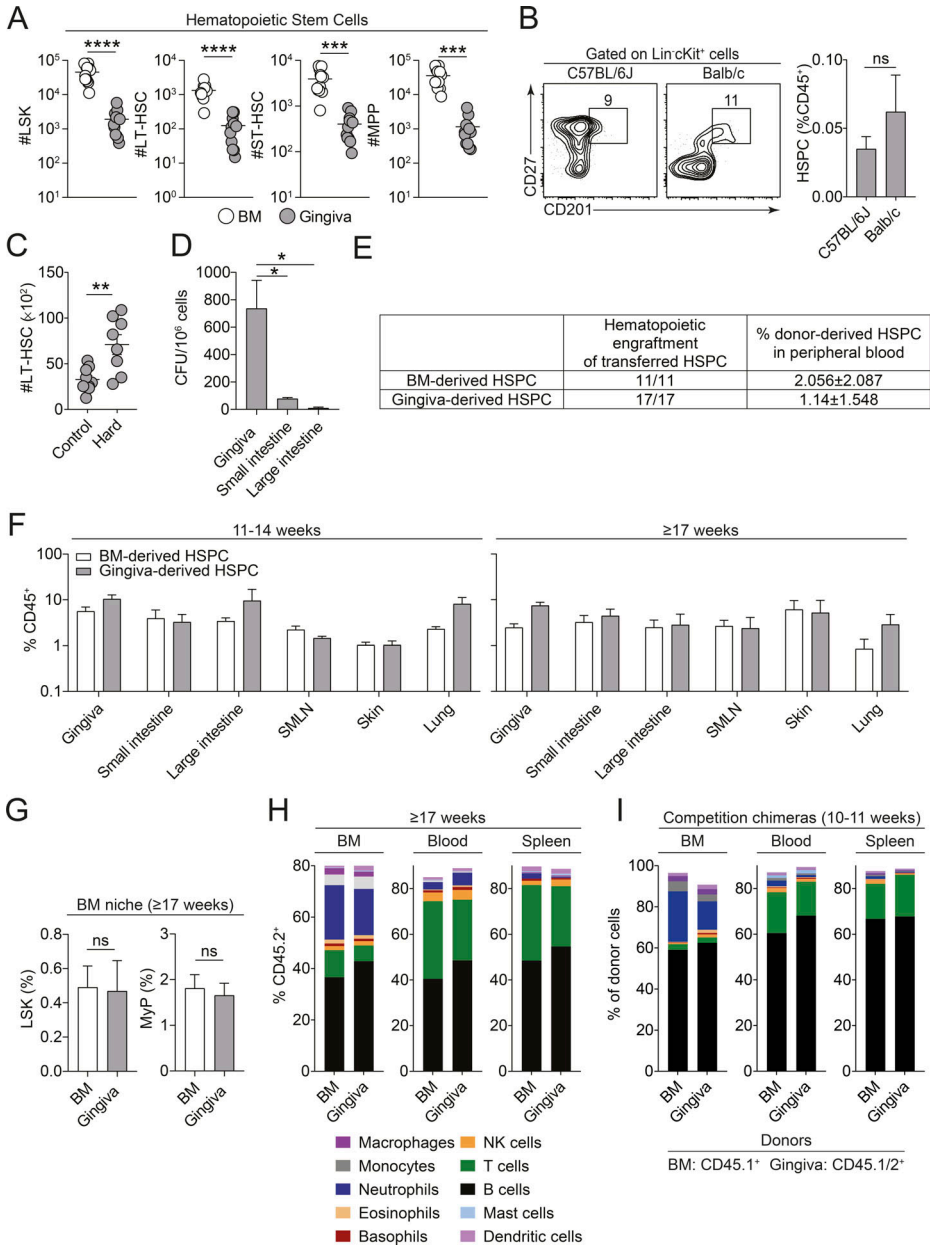

	Hematopoietic engraftment of transferred HSPC	% donor-derived HSPC in peripheral blood
BM-derived HSPC	11/11	2.056±2.087
Gingiva-derived HSPC	17/17	1.14±1.548

Figure S2. **HSPCs are present in gingival tissue and exhibit hematopoietic activity. (A)** Number of HSCs in the BM per femur and gingiva. *n* = 12 mice per group pooled from four independent experiments. **(B)** Left: Representative FACS plots identify HSPCs in the gingiva of C57BL/6J and Balb/c mice. Numbers indicate frequencies of HSPCs among Lin⁻cKit⁺ cells. Right: Frequencies of HSPCs in the gingiva of C57BL/6J and Balb/c mice expressed as a percentage of total CD45⁺ cells. *n* = 4–6 per group. Lin = CD3ε, TCR-β, CD19, B220, NK1.1, Ter119, Siglec F, Ly6G, FcεR1α, CD11b, CD11c, and Ly6C. **(C)** Absolute number of LT-HSCs from mice fed normal or a hardened chow diet for 8 wk. *n* = 8–9 mice per group pooled from three independent experiments. **(D)** CFU activity from MethoCult cultures of gingiva and small and large intestines. *n* = 2–6 per group pooled from four experiments. **(E–H)** CD45.1/2 hosts were sublethally irradiated and received equal numbers of LSK + MyPs FACS-sorted from the gingiva or BM of CD45.2 mice alongside total BM cells from CD45.1 mice. **(E)** Table showing numbers of chimera hosts into which HSPCs from either BM or gingiva were transferred and details of engraftment of the transferred HSPCs. **(F)** Bar graph showing frequencies of BM and gingiva HSPC-derived progeny in the indicated tissues expressed as a percentage of the total CD45⁺ population examined 11–14 wk (left) or ≥17 wk (right) after reconstitution. *n* = 3–6 mice per group from two independent experiments. SMLN, submandibular lymph node. **(G)** Bar graphs show frequencies of BM LSKs and MyPs that were derived from BM-HSPCs (white bars) or gingiva-HSPCs (gray bars) examined ≥17 wk after reconstitution. Data expressed as a percentage of total donor HSPC-derived cells. *n* = 5–8 mice per group from three independent experiments. **(H)** Lineage output of BM and gingiva HSPC-derived progeny in the BM, blood, and spleen at ≥17 wk after reconstitution, expressed as a percentage of total donor HSPC-derived cells. *n* = 7–12 mice per group from three independent experiments. **(I)** Equal numbers of LSK + MyPs were sorted from the BM of CD45.1 mice and gingiva of CD45.1/2 mice and transferred into sublethally irradiated CD45.2 hosts who also received total CD45.2 BM cells. Mice were reconstituted for 10–11 wk following which BM- and gingiva-derived cells were analyzed by FACS. Lineage output of BM and gingiva HSPC-derived progeny in the BM, blood, and spleen expressed as a percentage of total donor HSPC-derived cells. *n* = 3–5 mice per group from two independent experiments. Data are presented as mean ± SEM, except in H and I, where mean frequencies of HSPC-derived progeny are plotted. Statistical comparisons were performed using an unpaired *t* test (D and G) with Welch's correction (A–C) and a two-way ANOVA with a Holm–Šídák post hoc test (F, H, and I); ****, P < 0.0001; ***, P < 0.001; **, P < 0.01; *, P < 0.05.

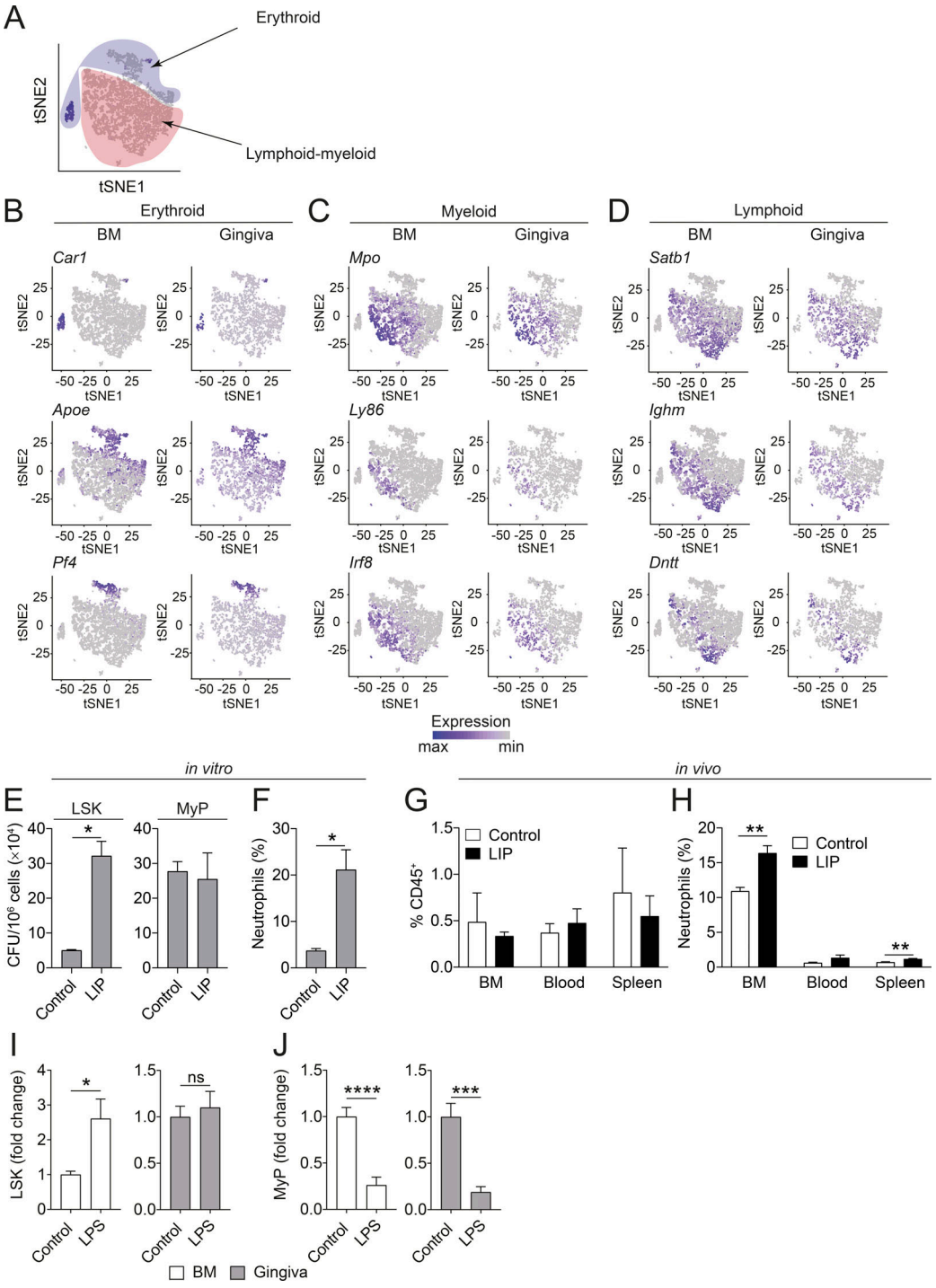

Figure S3. **HSPCs in the gingiva and BM show altered responsiveness to inflammatory signals. (A)** Single-cell RNA-seq analysis of total LSK + MyP cells isolated by FACS from the gingiva and BM showing the annotation of identified lineages on the core model. **(B–D)** tSNE plots show the expression of erythroid (B), myeloid (C), and lymphoid (D) lineage-associated gene transcripts projected onto the core model. **(E–H)** LIP was induced in cohorts of mice, at day 10 after ligature placement, and gingiva HSPCs were FACS sorted from the gingiva. HSPCs were FACS sorted from naive gingiva as a control. **(E)** CFU activity from MethoCult cultures of sorted LSK and MyP. **(F)** Quantification of neutrophil output from MethoCult cultures of LSK sorted from control and LIP gingiva, as assessed by flow cytometry. n = 2 from two independent experiments. **(G and H)** Total HSPCs (LSK + MyP) were sorted from the gingiva of control or LIP CD45.1/2 mice and transferred into sublethally irradiated CD45.2 hosts along with total BM cells from CD45.1 mice. Mice were examined 10–11 wk after reconstitution. **(G)** Quantification of HSPC-derived cellular progeny in indicated tissues expressed as a percentage of the total CD45⁺ population. **(H)** Neutrophil output as a proportion of CD45⁺ cells from control or LIP gingival HSPCs in the BM, blood, and spleen expressed as a percentage of total donor HSPC-derived cells. n = 3–4 per group from two independent experiments. **(I and J)** Fold-change in the percentages of LSK (I) and MyP (J) in the gingiva and BM 18 h following i.p. administration of 5 µg LPS. n = 6–9 mice per group pooled from three experiments. Data are presented as the mean ± SEM. Statistical comparisons were performed using an unpaired t test (E and F) with Welch's correction (H–J) and a two-way ANOVA with a Holm–Šídák post hoc test (G); ****, P < 0.0001; ***, P < 0.001; **, P < 0.01; *, P < 0.05.